日本磁気学会
ISSN 2432-0250
Journal of the Magnetics Society of Japan
Electronic Journal URL: https://www.jstage.jst.go.jp/browse/msjmag

Vol.47 No.5　2023

Journal

JOURNAL OF THE MAGNETICS SOCIETY OF JAPAN

Vol.47 No.5 2023

日本磁気学会

ISSN 2432-0250

HP: http://www.magnetics.jp/ e-mail: msj@bj.wakwak.com

Electronic Journal: http://www.jstage.jst.go.jp/browse/msjmag

TOEI

世界初！
高温超電導型VSM

新製品

世界初*、高温超電導マグネットをVSMに採用することで
測定速度 当社従来機1/20を実現。
0.5mm cube磁石のBr, HcJ高精度測定が可能となりました。

*2014年7月 東英工業調べ

測定結果例

高温超電導VSMによるNdFeB(sint.) 0.5mm cube BHカーブ

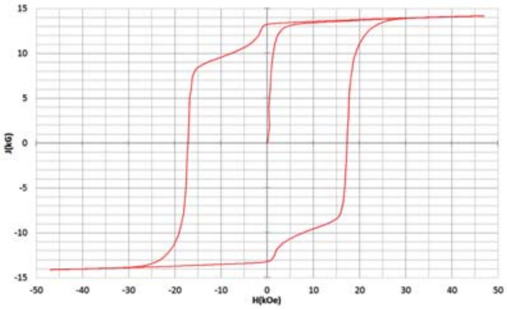

磁化測定レンジ：0.2emu
Br = 13.2kG　HcJ = 17.2kOe

高温超電導VSMによるNdFeB(sint.) 1mm cube BHカーブ

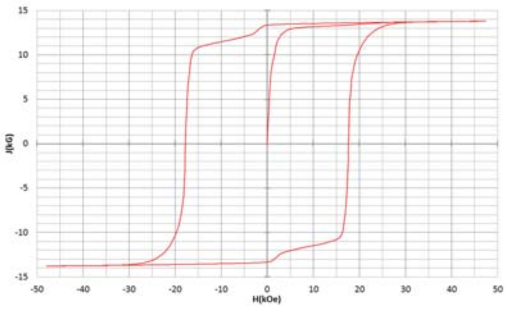

磁化測定レンジ：2emu
Br = 13.3kG　HcJ = 17.7kOe

高温超電導VSMによるNdFeB(sint.) 4mm cube BHカーブ

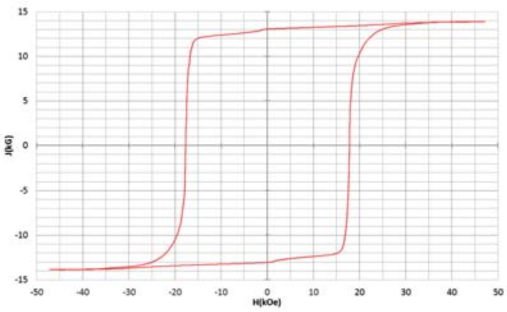

磁化測定レンジ：100emu
Br = 13.1kG　HcJ = 17.8kOe

高速測定を実現

高温超電導マグネット採用により、高速測定を実現しました。Hmax= 5Tesla, Full Loop 測定が2分で可能です。
(当社従来機：Full Loop測定 40分)

小試料のBr,HcJ高精度測定

0.5mm cube磁石のBr,HcJ高精度測定ができ、表面改質領域を切り出しBr,HcJの強度分布等、微小変化量の比較測定が可能です。
また、試料の加工劣化の比較測定が可能です。

試料温度可変測定

−50℃～+200℃温度可変UNIT（オプション）

磁界発生部の小型化

マグネットシステム部寸法：0.8m×0.3m×0.3m

TOEI 東英工業株式会社
http://www.toeikogyo.co.jp

〒194-0035 東京都町田市忠生1-8-13
TEL：042-791-1211　FAX：042-792-0490
E-mail：sales@toeikogyo.co.jp

Journal of the Magnetics Society of Japan

Vol. 47, No. 5

Electronic Journal URL: https://www.jstage.jst.go.jp/browse/msjmag

CONTENTS

J. Magn. Soc. Jpn., **47**, 128-132 (2023)

<Paper>

Approximate Equation for Energy Barrier in Magnetic Recording

T. Kobayashi and I. Tagawa*

Graduate School of Engineering, Mie Univ., *1577 Kurimamachiya-cho, Tsu 514-8507, Japan*

*Electrical and Electronic Engineering, Tohoku Institute of Technology, *35-1 Yagiyama-Kasumicho, Sendai 982-8577, Japan*

We derive an approximate energy barrier equation considering its adaptation to our model calculation employing the Néel-Arrhenius model with the Stoner-Wohlfarth grain or dot in magnetic recording. First, we calculate the energy barrier as a function of magnetic field by employing a numerical calculation for an angle of 0 to 180 deg between an easy axis and the magnetic field. This relation is represented by an approximate equation for an angle of 0 to 90 deg, taking account of Pfeiffer's approximation for an angle of 90 to 180 deg. Next, the shape anisotropy energy for a cuboid or cylinder is also represented by an approximate equation, since the energy barrier is a function of the shape anisotropy energy.

Key words: energy extremum, energy barrier, demagnetizing factor, shape anisotropy energy

1. Introduction

The challenges facing the design of magnetic recording (MR) media are
(1) information stability during 10 years of archiving, known as the $K_{\rm u}V/(kT)$ problem[1],
(2) information stability in an adjacent track during writing, known as the adjacent track interference (ATI) problem, and
(3) the writing field dependence of the bit error rate, namely writability.
These three subjects, which are in a trade-off relationship, must be dealt with simultaneously. Micromagnetic calculation is useful for examining (2) in shingled MR (SMR) and (3). However, this is not practical due to the long calculation time required for subjects (1) and (2) in conventional MR (CMR) because of the 10^3-10^4 times rewrite in the adjacent track. We have proposed a model calculation employing the Néel-Arrhenius model with the Stoner-Wohlfarth grain or dot. This model is applicable to all three subjects[2] including SMR and CMR. In our model calculation, the energy barrier is important. We have dealt with the writing field perpendicular to the medium plane. However, to examine the effect of oblique writing fields on ATI problem, the value of the energy barrier is necessary for angles of 90 to 180 deg between the easy axis and the magnetic field. Many approximations for the energy barrier have been proposed[3-6] for angles of 90 to 180 deg. Furthermore, to examine the effect of oblique writing fields on writability, the energy barrier for an angle of 0 to 90 deg is also necessary in our model calculation, since we need the probability for each attempt where the magnetization and writing field change from parallel to antiparallel[7]. Many design parameters are related to each other in a complex manner for heat-assisted magnetic recording (HAMR), since HAMR is a recording technique in which the medium is heated to reduce coercivity during the writing period. A feature of our model calculation is that it is easy to grasp the physical implication of writing process in HAMR and the calculation time is short. As far as we know, this approximate equation has not been obtained.

In this paper, we calculate the energy barrier as a function of magnetic field by employing a numerical calculation for angles of 0 to 180 deg, and propose an approximate energy barrier equation for angles of 0 to 90 deg considering its adaptation to our model calculation, taking account of Pfeiffer's approximation[5] for angles of 90 to 180 deg. We also mention an approximate equation for shape anisotropy energy, since the energy barrier is also a function of the shape anisotropy energy. For granular media with grains of various shapes, it takes a long time to calculate numerically the shape anisotropy energy of each grain. If the approximate equation is applied, a significant reduction in calculation time can be expected.

Corresponding author: T. Kobayashi (e-mail: kobayasi @phen.mie-u.ac.jp).

2. Calculation Method and Results

2.1 Energy extremum

We define an angle θ between an easy axis and a magnetization vector $\boldsymbol{M}$ (magnitude M), and ϕ

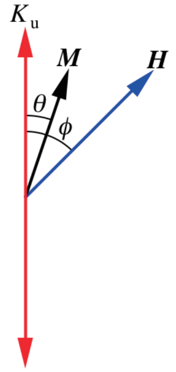

Fig. 1 Definition of angles of magnetization $\boldsymbol{M}$ and external magnetic field $\boldsymbol{H}$ vectors.

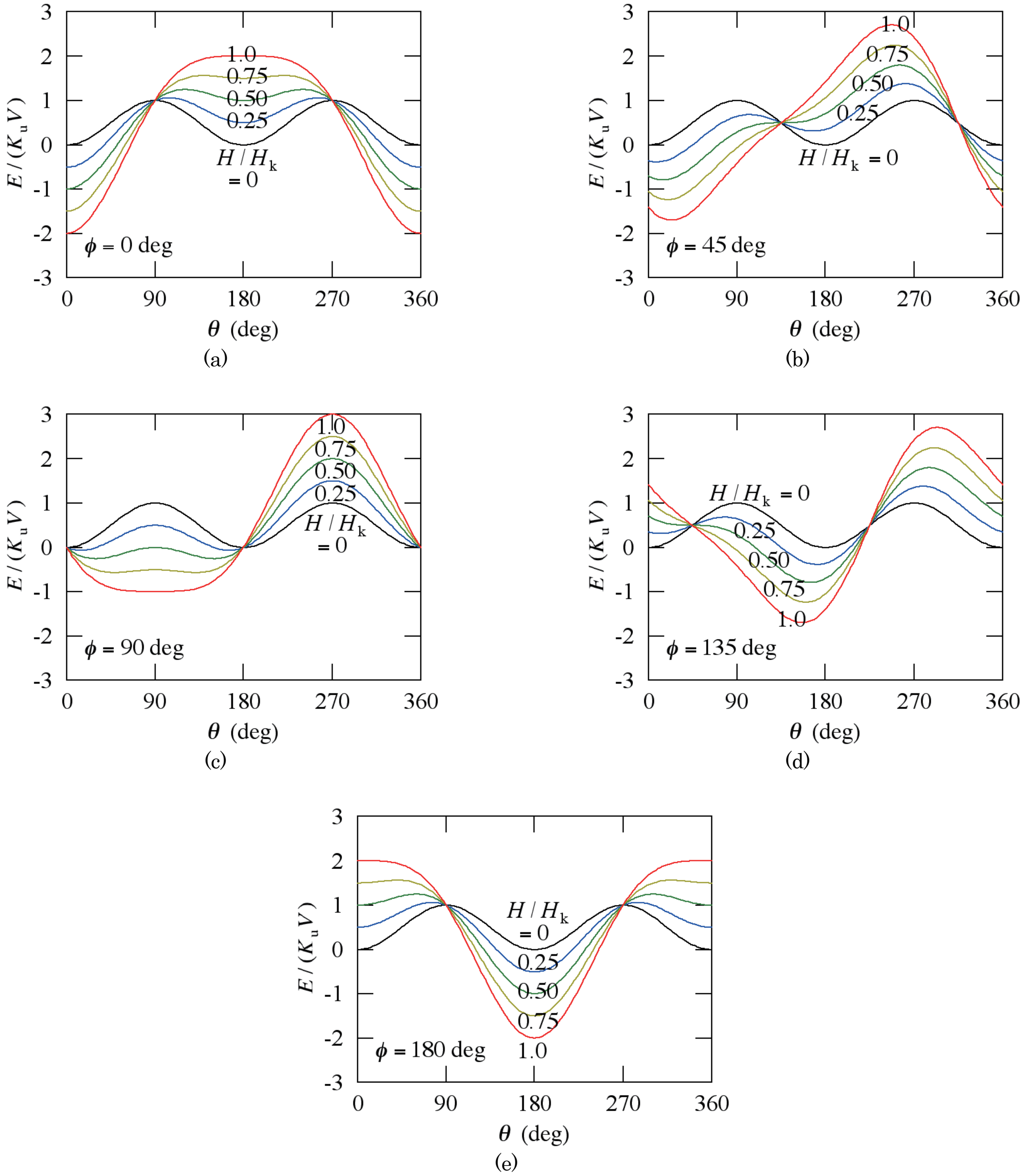

Fig. 2 Normalized energy $E/(K_uV)$ as a function of magnetization angle θ for various normalized fields H/H_k where ϕ is the field angle. (a) $\phi = 0$, (b) 45, (c) 90, (d) 135, and (e) 180 deg.

between an easy axis and an external magnetic-field vector $\boldsymbol{H}$ (magnitude H) as shown in Fig. 1. The summation $E = E_Z + E_a$ of Zeeman energy $E_Z = -\boldsymbol{M}\cdot\boldsymbol{H}V$ and anisotropy energy $E_a = K_uV\sin^2\theta$ is given by

$$E = -\boldsymbol{M}\cdot\boldsymbol{H}\,V + K_uV\sin^2\theta$$
$$= -M_sHV\cos(\theta-\phi) + K_uV\sin^2\theta, \qquad (1)$$

where K_u and V are the anisotropy constant and grain or dot volume, respectively. The $E/(K_uV)$ value is used below instead of E as

$$\frac{E}{K_uV} = -2\frac{H}{H_k}\cos(\theta-\phi) + \sin^2\theta, \qquad (2)$$

where H_k is an anisotropy field defined by $2K_u/M_s$.

Figure 2 shows the normalized energy $E/(K_uV)$ as a function of θ for various normalized fields H/H_k. When (a) $\phi = 0$ deg, there are two local minima and two local maxima between $0 \le \theta < 360$ deg for $0 \le H/H_k < 1.0$, and two θ values of 0 and 180 deg at which the magnetization is stable. For $H/H_k = 1.0$, the number of local minima decreases to one at $\theta = 0$ deg, and the magnetization switches from $\theta = 180$ to 0 deg. When (b)

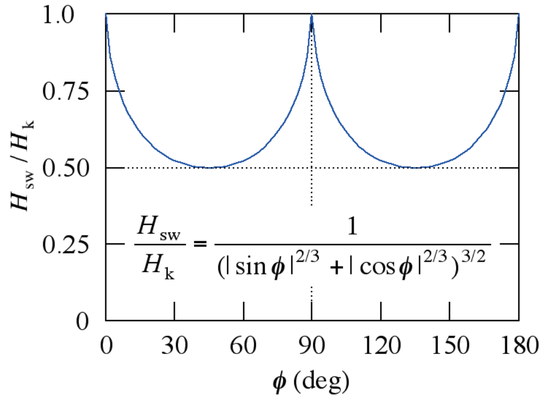

Fig. 3 Normalized switching field $H_{\mathrm{sw}}/H_{\mathrm{k}}$ as a function of field angle ϕ[3,4].

$\phi = 45$ deg, there are also two local minima and two local maxima between $0 \le \theta < 360$ deg for $0 \le H/H_{\mathrm{k}} < 0.5$, and the number of local minima decreases to one, and magnetization switching occurs at $H/H_{\mathrm{k}} = 0.5$. The switching field H_{sw} is a function of ϕ, which is well known[3,4] as

$$\frac{H_{\mathrm{sw}}}{H_{\mathrm{k}}} = \frac{1}{(|\sin\phi|^{2/3}+|\cos\phi|^{2/3})^{3/2}}. \qquad (3)$$

This relation is shown in Fig. 3, for example $H_{\mathrm{sw}}/H_{\mathrm{k}} = 1.0$ at $\phi = 0$ deg, and $H_{\mathrm{sw}}/H_{\mathrm{k}} = 0.50$ at $\phi = 45$ deg.

2.2 Energy barrier

When there are two local minima E_0 and one local maximum E_1 between $0 \le \theta \le 180$ deg, the energy barrier is given by the difference between E_1 and E_0 with a smaller θ value. It is well known that the $(E_1 - E_0)/(K_{\mathrm{u}}V)$ values for ϕ = 0, 90, and 180 deg can be calculated analytically as

$$\frac{E_1-E_0}{K_{\mathrm{u}}V} = \left(1 + \frac{H}{H_{\mathrm{k}}}\right)^2, \text{ and} \qquad (4)$$
$(\phi = 0$ deg)

$$\frac{E_1-E_0}{K_{\mathrm{u}}V} = \left(1 - \frac{H}{H_{\mathrm{k}}}\right)^2. \qquad (5)$$
$(\phi = 90$ and 180 deg)

We can obtain the $E_1 - E_0$ values for all $0 \le \phi \le 180$ deg values by employing a numerical calculation as shown by open circles in Fig. 4. For $H/H_{\mathrm{k}} > H_{\mathrm{sw}}/H_{\mathrm{k}}$, there exists no $E_1 - E_0$, since there is one local minimum E_0 between $0 \le \theta \le 180$ deg.

If this relation can be represented by an approximate equation, it will be convenient for various analyses, especially for our model calculation[7], since the numerical calculation becomes unnecessary and the calculation time is shortened. When $90 \le \phi \le 180$ deg, it has been reported by Pfeiffer[5] as

$$\frac{E_1-E_0}{K_{\mathrm{u}}V} = \left(1 - \frac{H/H_{\mathrm{k}}}{H_{\mathrm{sw}}/H_{\mathrm{k}}}\right)^x, \text{ where}$$
$(0 \le H/H_{\mathrm{k}} \le H_{\mathrm{sw}}/H_{\mathrm{k}})$

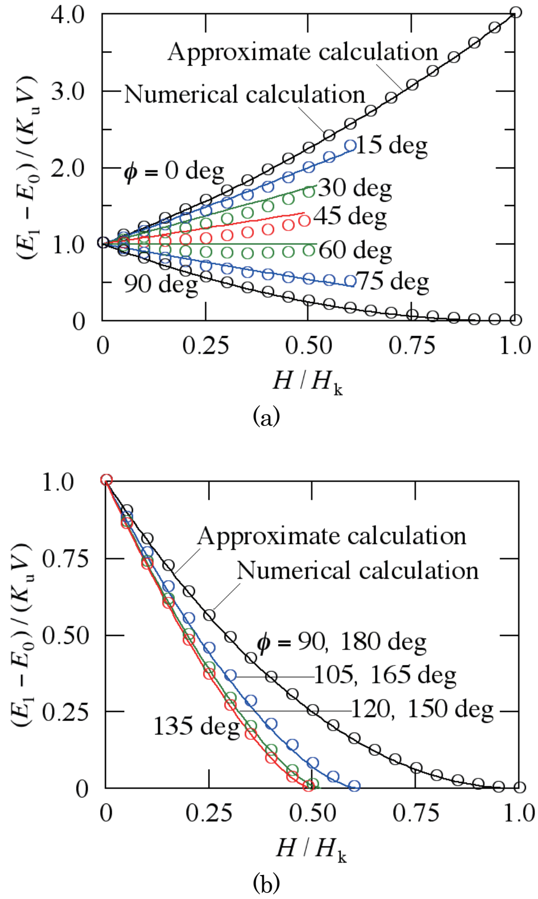

Fig. 4 Normalized energy barrier $(E_1 - E_0)/(K_{\mathrm{u}}V)$ obtained by employing numerical and approximate calculations as a function of normalized field H/H_{k} for (a) $0 \le \phi \le 90$ deg and (b) $90 \le \phi \le 180$ deg[5].

$$x = 0.86 + 1.14(H_{\mathrm{sw}}/H_{\mathrm{k}}). \qquad (6)$$

The result calculated using Eq. (6) is shown by solid lines in Fig. 4 (b). A comparison reveals fairly good agreement between the numerical and approximate calculations.

We referred to Eq. (6) for $0 \le \phi \le 90$ deg as

$$\frac{E_1-E_0}{K_{\mathrm{u}}V} = \left(1 + f(\phi)\frac{H/H_{\mathrm{k}}}{H_{\mathrm{sw}}/H_{\mathrm{k}}}\right)^x. \qquad (7)$$

Taking account of $f(\phi) = +1$ for $\phi = 0$ deg, $f(\phi) = -1$ for $\phi = 90$ deg, and that the $E_1 - E_0$ value is almost independent of H/H_{k} for $\phi = 60$ deg as shown in Fig. 4 (a), we adopted the following equation as $f(\phi)$.

$$f(\phi) = 2\left(\cos\phi - \frac{1}{2}\right). \qquad (8)$$

Next, in the following equation, we searched for the a value that fitted the numerical calculation and obtained $a = 2.0$.

$$\frac{E_1-E_0}{K_{\mathrm{u}}V} = \left(1 + 2\left(\cos\phi - \frac{1}{2}\right)\frac{H/H_{\mathrm{k}}}{H_{\mathrm{sw}}/H_{\mathrm{k}}}\right)^x, \text{ where}$$
$$x = (2 - a) + a(H_{\mathrm{sw}}/H_{\mathrm{k}}). \qquad (9)$$

As a result, we derived the following approximate equation for $0 \le \phi \le 90$ deg.

$$\frac{E_1 - E_0}{K_u V} = \left(1 + 2\left(\cos\phi - \frac{1}{2}\right)\frac{H/H_k}{H_{sw}/H_k}\right)^x, \text{ where}$$
$$(0 \le H/H_k \le H_{sw}/H_k)$$
$$x = 2.0(H_{sw}/H_k). \quad (10)$$

Equation (10) agrees with Eq. (4), since $f(\phi)H/H_{sw} = +H/H_k$ and $x = 2$ for $\phi = 0$ deg, and agrees with Eq. (5), since $f(\phi)H/H_{sw} = -H/H_k$ and $x = 2$ for $\phi = 90$ deg. The calculated result obtained using Eq. (10) is shown by solid lines in Fig. 4 (a). The relative error is between +15 to −10 %. Therefore, Eqs. (6) and (10) have a sufficiently good accuracy for application to model calculations.

If we need to take the magneto-static and exchange-coupling energies from the surrounding grains or dots into account, they are incorporated into $\boldsymbol{H}$ as vectors, since they have the same interaction energy as E_Z.

2.3 Shape anisotropy energy

The energy barrier is a function of the shape anisotropy energy. The approximate equation for a demagnetizing factor will also be convenient. A demagnetizing factor has been calculated for oblate and prolate spheroids[8].

We assumed a grain or a dot to be a cuboid with a size D_x for the down-track direction, D_y for the cross-track direction, and height h where the volume V is $D_x \times D_y \times h$. The demagnetizing field H_d at the center of the grain or dot for $\theta = 0$ deg is calculated with

$$H_d = 8M_s \arctan\left(\frac{D_x D_y}{h\sqrt{D_x^2 + D_y^2 + h^2}}\right) = M_s N_z, \quad (11)$$

where N_z is the demagnetizing factor along the z axis. The shape anisotropy constant K_{shape} is approximately expressed[9] by

$$K_{shape} = \frac{(4\pi - 3N_z)M_s^2}{4}. \quad (12)$$

If $h \ll D_x$ and D_y, N_z and K_{shape} become 4π and $-2\pi M_s^2$, respectively. When cubic $D_x = D_y = h$, N_z and K_{shape} become $4\pi/3$ and 0, respectively.

Similarly, if a cylinder, whose diameter and height are D and h, respectively, is assumed, the H_d value at the center is calculated by

$$H_d = 4\pi M_s\left(1 - \frac{h}{\sqrt{D^2 + h^2}}\right) = M_s N_z. \quad (13)$$

If $h \ll D$, N_z becomes 4π.

The $N_z/(4\pi)$ and $K_{shape}/(2\pi M_s^2)$ values as a function of height $h/$(diameter or width D) are shown in Fig. 5 (a) and (b), respectively. The results for cuboid and cylinder approximations are fairly similar to the experimental result for a rod[8] and to the calculation results for oblate ($0.1 < h/D < 1$) and prolate ($1 < h/D < 10$) spheroids[8].

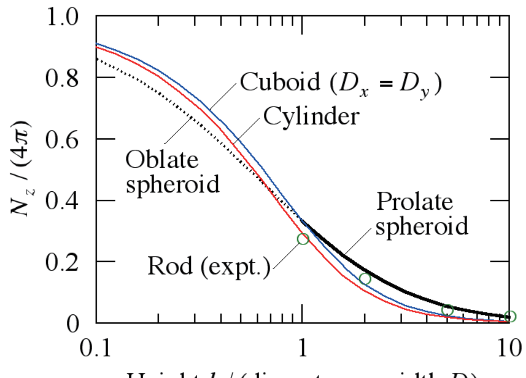

(a)

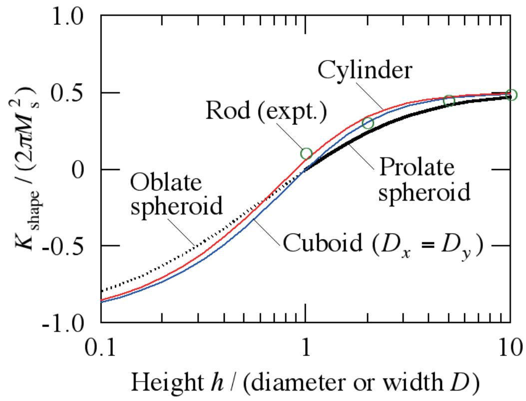

(b)

Fig 5 (a) Demagnetizing factor $N_z/(4\pi)$ and (b) shape anisotropy constant $K_{shape}/(2\pi M_s^2)$ as a function of height $h/$(diameter or width D). The $N_z/(4\pi)$ values for a rod (experimental) and spheroids are previously reported values[8].

For the spheroid model, the equation for N_z must be changed according to the h/D value. The cuboid and cylinder models are simple and it is easy to grasp the physical implication. Although Eqs. (11) and (13) are approximations at the particle center, they are sufficient for application to model calculations.

Since the shape anisotropy energy E_{shape} has the same self-energy as E_a, E_a and E_{shape} can be considered together.

$$E_a + E_{shape} = K_u V \sin^2\theta + K_{shape} V \sin^2\theta$$
$$= \left(K_u + \frac{(4\pi - 3N_z)M_s^2}{4}\right) V \sin^2\theta. \quad (14)$$

If we put

$$K_{ueff} = K_u + \frac{(4\pi - 3N_z)M_s^2}{4}, \text{ and} \quad (15)$$

$$H_{keff} = \frac{2K_{ueff}}{M_s}, \quad (16)$$

the following equation can be obtained instead of Eq. (2).

$$\frac{E}{K_{ueff}V} = -2\frac{H}{H_{keff}}\cos(\theta - \phi) + \sin^2\theta. \quad (17)$$

When K_{shape} is considered, K_{u} and H_{k} can be regarded as K_{ueff} and H_{keff}, respectively.

4. Conclusions

We proposed an approximate equation for the energy barrier for angles of 0 to 90 deg between the easy axis and the magnetic field, taking account of Pfeiffer's approximation for angles of 90 to 180 deg. The relative error is between +15 to −10 %. The equation we derived has a sufficiently good accuracy for application to model calculations. We also derived approximate equations for the shape anisotropy energy of cuboids or cylinders, since the energy barrier is a function of the shape anisotropy energy. Although it is an approximate equation at the particle center, it is sufficiently effective for application to model calculations.

The adoption of this approximation for angles of 0 to 180 deg to our model calculation is a subject for future study.

Acknowledgement We acknowledge the support of the Advanced Storage Research Consortium (ASRC), Japan.

References

1) S. H. Charap, P. -L. Lu, and Y. He: *IEEE Trans. Magn.*, **33**, 978 (1997).
2) T. Kobayashi, Y. Nakatani, and Y. Fujiwara: *J. Magn. Soc. Jpn.*, **47**, 1 (2023).
3) R. H. Victora: *Phys. Rev. Lett.*, **63**, 457 (1989).
4) H. N. Bertram and H. J. Richter: *J. Appl. Phys.*, **85**, 4991 (1999).
5) H. Pfeiffer, *phys. status solidi* (a), **118**, 295 (1990).
6) W. Wernsdorfer, E. B. Orozco, K. Hasselbach, A. Benoit, B. Barbara, N. Demoncy, A. Loiseau, H. Pascard, and D. Mailly: *Phys. Rev. Lett.*, **78**, 1791 (1997).
7) T. Kobayashi, Y. Nakatani, and Y. Fujiwara: *J. Magn. Soc. Jpn.*, **42**, 127 (2018).
8) R. M. Bozorth: *Ferromagnetism* (D. van Nostrand Co., 1951).
9) K. Takanashi: *Jikikogaku Nyumon* (in Japanese), p. 63 (Kyoritsu Shuppan, Tokyo, 2008).

Received Apr. 11, 2023; Revised May 19, 2023; Accepted Jun. 22, 2023

INDEX

J. Magn. Soc. Jpn., **47**, 133-136 (2023) <Letter>

Rectification effect of non-centrosymmetric Nb/V/Ta superconductor

Ryo Kawarazaki[1], Ryo Iijima[1], Hideki Narita[1], Ryusuke Hisatomi[1,2], Yoichi Shiota[1,2],
Takahiro Moriyama[1,2,*], and Teruo Ono[1,2,3]
[1]Institute for Chemical Research, Kyoto University, *Gokasho, Uji, Kyoto 611-0011, Japan*
[2]Center for Spintronics Research Network, Institute for Chemical Research, Kyoto University,
Gokasho, Uji, Kyoto, 611-0011, Japan
[3]Center for Spintronics Research Network (CSRN), Graduate School of Engineering Science, Osaka University,
1-3 Machikaneyama-cho Toyonaka, Osaka 560-8531, Japan
*Current address: Department of Materials Physics, Nagoya University

The superconducting diode effect in which electrical resistance is zero in only one direction has recently been reported in superconductors without inversion symmetry. Previous studies investigated the nonreciprocity of the critical current, but little has been known about the rectification effect when AC currents are applied. Herein, we examined the rectification characteristics of a non-centrosymmetric Nb/V/Ta artificial superlattice under AC currents. The rectification strength can be modulated by an applied magnetic field, and its polarity can be tuned by the magnetic field. Furthermore, we find that the magnetic field dependence of the rectification is different from that of the nonreciprocal critical current.

Key words: superconducting diode, rectification, artificial superlattice, inversion symmetry breaking

1. Introduction

Rectification, the conversion of a bidirectional current into a unidirectional current, is an essential process in modern electronics. The electronic devices that enable rectification are called diodes and are widely used to convert alternating current (AC) to direct current (DC), protect electrical circuits from overvoltage, and detect electromagnetic radiation. Conventional diodes, composed of different types of semiconductors connected to form a p-n junction, exhibit a low resistance in one direction and a high resistance in the other direction. Although the diode effect forms the basis for numerous electronic components, energy loss is inevitable in the semiconductor diodes due to their finite resistance. Therefore, superconducting diodes with zero electrical resistance in one direction hold great promise for practical use. Wakatsuki *et al.* demonstrated that the nonreciprocal resistance in a low-symmetry 2D material increases by orders of magnitude in the fluctuating regime of superconductivity as compared to the normal conduction state.[1)] In addition, a rectification effect has been detected in superconducting thin films designed to control the magnetic fluxes that pierce the superconductor.[2)-10)] However, such superconducting diode effect can only manifest itself when the superconductors have a non-zero resistance.

We fabricated an artificial superlattice consisting of stacked alternating layers of Nb, V, and Ta, and demonstrated an ideal superconducting diode that has zero resistance in only one direction.[11)-12)] Stimulated by our experiment, theoretical groups proposed an intrinsic mechanism to cause the superconducting diode effect.[13)-14)] They suggested that the Cooper pair of a superconductor without inversion symmetry acquires a finite momentum under an in-plane magnetic field, and that the depairing current, the upper limit of the critical current, is non-equivalent in the directions parallel and anti-parallel to its momentum. Subsequently, several experimental results on the superconducting diode effect using materials without inversion symmetry have been reported.[15)-18)] In the study of the superconducting diode effect exhibited by non-centrosymmetric superconductors, the nonreciprocity of the critical current has been investigated so far, but for its application, it is necessary to investigate the rectification characteristics when an AC current is applied. In this study, we examined the rectification effect when an AC current was injected into a non-centrosymmetric Nb/V/Ta artificial superlattice.

2. Experimental Results

2.1 Nonreciprocal Critical Current

We used the same [Nb(1.0 nm)/V(1.0 nm)/Ta(1.0 nm)]$_{40}$ superlattice used in Ref. 19. Figure 1(a) shows a photograph of the device and a schematic diagram of the experimental setup. The transport measurement was performed in a four-terminal configuration by using a nanovoltmeter (Keithley2182A) and a current source

Corresponding author:
T. Ono (e-mail: ono@scl.kyoto-u.ac.jp).

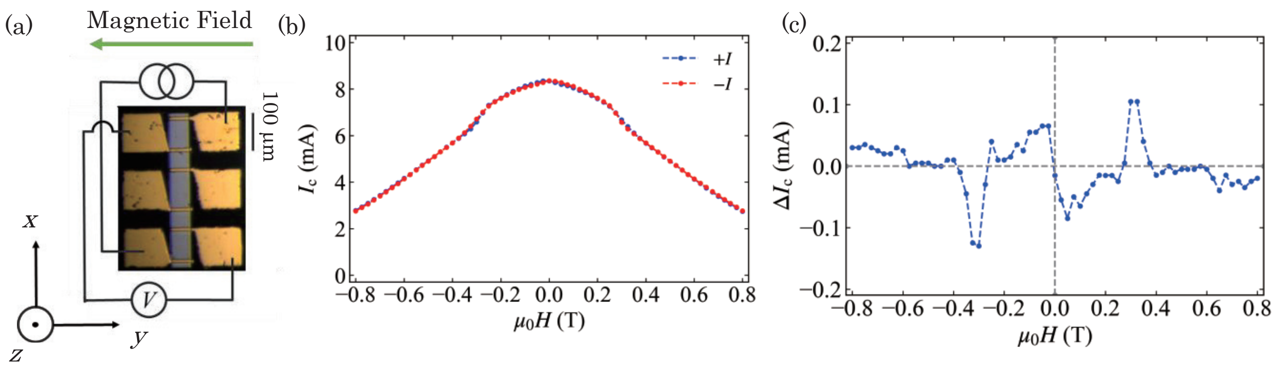

Fig. 1 (a) Photomicrograph of device and experimental setup. Current was applied in x direction and magnetic field in y direction. z-axis is polar axis of $[Nb/V/Ta]_{40}$ artificial superlattice. (b) Magnetic field dependence of positive critical current I_{c+} and negative critical current I_{c-}. (c) Magnetic field dependence of nonreciprocal component ΔI_c (= $|I_{c+}| - |I_{c-}|$). Temperatures in (b) and (c) are both 2 K.

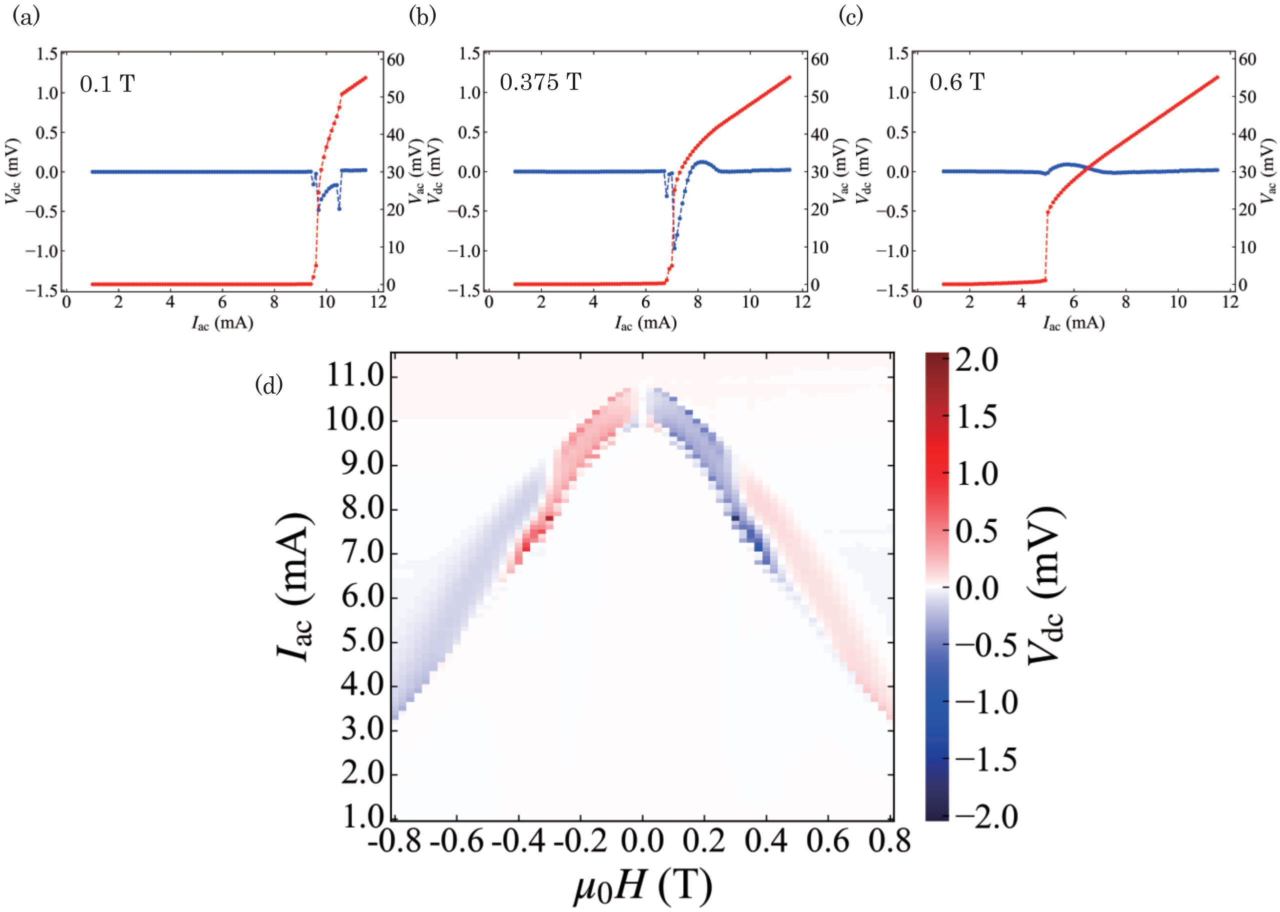

Fig. 2 (a-c) AC current dependence of rectification voltage (blue dots) and AC voltage (red dots) when in-plane magnetic field was applied orthogonal to current direction. (a) 0.1 T, (b) 0.375 T, and (c) 0.6 T were applied. (d) Color plot of rectification voltage with respect to AC current and magnetic field. Temperatures in (a)-(d) are all 2 K.

(Yokogawa7651). The temperature and magnetic field were controlled using a commercial refrigerator (Quantum Design, Physical Property Measurement System). The superconducting transition temperature was 3.3 K under a zero magnetic field. We measured the critical current by increasing the current under a constant in-plane magnetic field orthogonal to the current direction. Figure 1(b) shows the magnetic field dependence of the critical current. The critical current were different whether the applied currents were positive or negative. Here, the nonreciprocal critical current ΔI_c, is defined as the difference between the critical current in the positive direction (I_c+) and that in the negative direction (I_c−). Figure 1(c) presents the magnetic field dependence of the nonreciprocal critical current. In the positive field region, the sign of the nonreciprocal critical current was negative below 0.275 T, positive between 0.275 and 0.375 T, and negative again above 0.375 T. This oscillating behavior of the nonreciprocal critical current is consistent with our previous report[20].

2.2 Rectification Effect

To probe the rectification effect, we investigated the magnetic field dependence of the rectification voltage under a sinusoidal AC current of 100 kHz. We injected AC currents into the device with an AC current source (Keithley 6221 AC and DC current source), and measured DC voltages with a nanovoltmeter (Keithley 2182A) and AC voltages with a multimeter (Keithley 2000). Figure 2(a) shows the change in DC voltage (blue dots) and AC voltage (red dots) as the AC current amplitude was increased under an in-plane magnetic field of 0.1 T. The rectification voltage appeared in close vicinity to the superconductor-to-metal transition. Figures 2(b) and 2(c) show the rectification voltage when magnetic fields of 0.375 T and 0.6 T were applied, respectively. We observed negative rectification voltage at 0.1 T, both positive and negative rectification voltage at 0.375 T, and positive voltage at 0.6 T. Furthermore, dip structures were observed in Fig. 2(a) and Fig. 2(b). Although the origin of the dip structures was not clear at this stage, one possibility can be the vortex ratchet motion reported in Ref. 2. To investigate the rectification effect in detail, we plotted the rectification voltage as a function of magnetic field and AC current amplitude in Fig. 2(d). Comparing Fig. 2(d) with Fig. 1(c), between 0 and 0.275 T, the sign of the rectification voltage was the same as that of the nonreciprocal critical current. At 0.325 T, where the sign of the nonreciprocal critical current was reversed to be positive, both positive and negative rectification voltages were observed. As the magnetic field was further increased to 0.6 T, where the sign of the nonreciprocal critical current was reversed again, the polarity of the rectification voltage was opposite to that of the nonreciprocal critical current. The inconsistency between the signs of the superconducting diode effect and the rectification voltage observed here could be due to the additional contributions of the dynamics of vortex or non-equilibrium quasiparticles driven by AC current. To elucidate the mechanism, it is necessary to further investigate the frequency dependence of the rectification effect.[21)-23)]

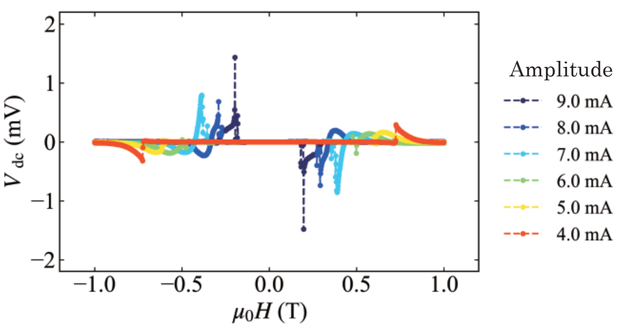

Fig. 3 Magnetic field dependence of rectification voltage when AC current amplitude was constant at 2 K.

In Fig. 2(d), we examined the rectification voltage when an AC current amplitude was increased under a constant magnetic field. To check the reproducibility, we also investigated the rectification voltage when a magnetic field was increased under a constant AC current amplitude. Figure 3 shows the magnetic field dependence of the rectification voltage when an AC current amplitude was increased from 4 to 9 mA. The polarity of the rectification was reversed as the AC current amplitude was increased, which was consistent with the experimental result of Fig. 2. We have reconfirmed the polarity reversal of the rectification effect induced by the magnetic field.

3. Conclusion

We have demonstrated the rectification effect of the Nb/V/Ta artificial superlattice superconductor. The rectification effect obtained here is expected to be observed in other non-centrosymmetric materials exhibiting the superconducting diode effect.

Acknowledgements This work was supported by JSPS KAKENHI Grant Numbers 22J21677, 21K18145, 21K13883, 20H05665, and the Collaborative Research Program of the Institute for Chemical Research, Kyoto University.

References

1) R. Wakatsuki, Y. Saito, S. Hoshino, Y. M. Itahashi, T. Ideue, M. Ezawa, Y. IWASA, and N. Nagaosa: *Sci. Adv.* **3**, e1602390 (2017).
2) J. Jiang, YL. Wang, M. V. Milošević, ZL. Xiao, F. M. Peeters, and QH. Chen: *Phys. Rev. B* **103**, 014502(2021).
3) YY. Lyu, J. Jiang, YL. Wang, ZL. Xiao, S. Dong, QH Chen, M. V. Milošević, H. Wang, R. Divan, J. E. Pearson, P. Wu, F. M.

Peeters, and WK. Kwok: *Nat Commun* **12**, 2703 (2021).
4) A. Yu. Aladyshkin, J. Fritzsche, and V. V. Moshchalkov: *Appl. Phys. Lett.* **94**, 222503 (2009).
5) W. Gillijns, A. V. Silhanek, V. V. Moshchalkov, C. J. Olson Reichhardt, and C. Reichhardt: *Phys. Rev. Lett.* **99**, 247002 (2007).
6) C. C. de Souza Silva, A. V. Silhanek, J. Van de Vondel, W. Gillijns, V. Metlushko, B. Ilic, and V. V. Moshchalkov: *Phys. Rev. Lett.* **98**, 117005 (2007).
7) C. de Souza Silva, J. Van de Vondel, M. Morelle, V. V. Moshchalkov: *Nature* **440**, 651–654 (2006).
8) D. E. Shalóm, and H. Pastoriza: *Phys. Rev. Lett.* **94**, 177001 (2005).
9) J. E. Villegas, S Savel'ev, F. Nori, E. M. Gonzalez, J. V. Anguita, R. Garcia, and J. L. Vicent: *Science* **302**, 1188–1191 (2003).
10) CS. Lee, B. Jankó, I. Derényi, A.-L. Barabási: *Nature* **400**, 337–340 (1999).
11) F. Ando, Y. Miyasaka, T. Li, J. Ishizuka, T. Arakawa, Y. Shiota, T. Moriyama, Y. Yanase, and Teruo Ono: *Nature* **584**, 373–376 (2020).
12) F. Ando, D. Kan, Y. Shiota, T. Moriyama, Y. Shimakawa, T. Ono: *J. Magn. Soc. Jpn* **43**, 17–20 (2019).
13) A. Daido, Y. Ikeda, and Y. Yanase: *Phys. Rev. Lett.* **128,** 037001(2022).
14) N. F. Q. Yuan, and L. Fu: *Proc. Natl. Acad. Sci.* **119**, e2119548119 (2022).
15) H. Narita, J. Ishizuka, R. Kawarazaki, D. Kan, Y. Shiota, T. Moriyama, Y. Shimakawa, A. V. Ognev, A. S. Samardak, Y. Yanase, and T. Ono: *Nat. Nanotechnol.* **17**, 823–828 (2022).
16) JX. Lin, P. Siriviboon, H.D. Scammell, S Liu, D. Rhodes, K. Watanabe, T. Taniguchi, J. Hone, M. S. Scheurer, and J.I.A. Li: *Nat. Phys.* **18**, 1221–1227 (2022).
17) L. Bauriedl, C. Bäuml, L. Fuchs, C. Baumgartner, N. Paulik, J. M. Bauer, KQ. Lin, J. M. Lupton, T. Taniguchi, K. Watanabe, C. Strunk, and Nicola Paradiso: *Nat Commun* **13**, 4266 (2022).
18) H. Wu, Y. Wang, Y. Xu, P. K. Sivakumar, C. Pasco, U. Filippozzi, S. S. P. Parkin, YJ Zeng, T. McQueen, and M. N. Ali*et*: *Nature* **604**, 653–656 (2022).
19) Y. Miyasaka, R. Kawarazaki, H. Narita, F. Ando, Y. Ikeda, R. Hisatomi, A. Daido, Y. Shiota, T. Moriyama, Y. Yanase, and T. Ono: *Appl. Phys. Express* **14**, 07300 (2021).
20) R. Kawarazaki, H. Narita, Y. Miyasaka, Y. Ikeda, R. Hisatomi, A. Daido, Y. Shiota, T. Moriyama, Y. Yanase, Alexey V. Ognev, Alexander S. Samardak, and T. Ono, *Appl. Phys. Express* **15**, 1130 (2022).
21) S. Chahid, S. Teknowijoyo, I. Mowgood, and A. Gulian: *Phys. Rev. B* **107**, 054506 (2023).
22) O. V. Dobrovolskiy, C. González-Ruano, A. Lara, R. Sachser, V. M. Bevz, V. A. Shklovskij, A. I. Bezuglyj, R. V. Vovk, M. Huth, and F. G. Aliev: *Commun Phys* **3**, 64 (2020).
23) D. Y. Vodolazov and F. M. Peeters: *Phys. Rev. B* **72**, 172508(2005).

Received May 10, 2023; Accepted May 31, 2023

Notice for Photocopying

複写をされる方へ

Journal of the Magnetics Society of Japan

Vol. 47 No. 5 (通巻第329号) 2023年9月1日発行

Vol. 47 No. 5 Published Sep. 1, 2023
by the Magnetics Society of Japan
Tokyo YWCA building Rm207, 1–8–11 Kanda surugadai, Chiyoda-ku, Tokyo 101–0062
Tel. +81–3–5281–0106 Fax. +81–3–5281–0107

Printed by JP Corporation Co., Ltd.
Sports Plaza building 401, 2–4–3, Shinkamata Ota-ku, Tokyo 144–0054
Advertising agency: Kagaku Gijutsu-sha

発行：(公社)日本磁気学会　101-0062　東京都千代田区神田駿河台 1-8-11　東京YWCA会館 207 号室
製作：ジェイピーシー　144-0054　東京都大田区新蒲田 2-4-3　スポーツプラザビル401　Tel.（03）6715-7915
広告取扱い：科学技術社　111-0052　東京都台東区柳橋 2-10-8　武田ビル4F　Tel.（03）5809-1132